Mon. Not. R. Astron. Soc. **376,** 1270–1284 (2007) doi:10.1111/j.1365-2966.2007.11517.x

Spitzer spectroscopy of carbon stars in the Small Magellanic Cloud

Eric Lagadec,[1⋆] Albert A. Zijlstra,[1] G. C. Sloan,[2] Mikako Matsuura,[1,3] Peter R. Wood,[4] Jacco Th. van Loon,[5] G. J. Harris,[6] J. A. D. L. Blommaert,[7] S. Hony,[8] M. A. T. Groenewegen,[7] M. W. Feast,[9] P. A. Whitelock,[9,10,11] J. W. Menzies[9] and M.-R. Cioni[12]

[1]*University of Manchester, School of Physics & Astronomy, PO Box 88, Manchester M60 1QD*
[2]*Department of Astronomy, Cornell University, 108 Space Sciences Building, Ithaca, NY 14853-6801, USA*
[3]*Division of Optical and IR Astronomy, National Astronomical Observatory of Japan, Osawa 2-21-1, Mitaka, Tokyo 181-8588, Japan*
[4]*Research School of Astronomy and Astrophysics, Australian National University, Cotter Road, Weston Creek, ACT 2611, Australia*
[5]*Astrophysics Group, School of Physical & Geographical Sciences, Keele University, Staffordshire ST5 5BG*
[6]*Department of Physics and Astronomy, University College London, Gower Street, London WC1E 6BT*
[7]*Instituut voor Sterrenkunde, K.U. Leuven, Celestijnenlaan 200 D, B-3001 Leuven, Belgium*
[8]*CEA, DSM, DAPNIA, Service d'Astrophysique, C.E. Saclay, F-91191 Gif-sur-Yvette Cedex, France*
[9]*Department of Astronomy, University of Cape Town, 7701 Rondebosch, South Africa*
[10]*South African Astronomical Observatory, PO Box 9, 7935 Observatory, South Africa*
[11]*NASSP, Department of Mathematics & Applied Mathematics, University of Cape Town, 7701 Rondebosch, South Africa*
[12]*Institute for Astronomy, University of Edinburgh, Royal Observatory, Blackford Hill, Edinburgh EH9 3HJ*

Accepted 2007 January 17. Received 2007 January 15; in original form 2006 October 31

ABSTRACT

We present *Spitzer Space Telescope* spectroscopic observations of 14 carbon-rich asymptotic giant branch (AGB) stars in the Small Magellanic Cloud (SMC). SiC dust is seen in most of the carbon-rich stars but it is weak compared to Large Magellanic Cloud (LMC) stars. The SiC feature is strong only for stars with significant dust excess, opposite to what is observed for Galactic stars. We argue that in the SMC, SiC forms at lower temperature than graphite dust, whereas in the Galaxy SiC and graphite condensate at more comparable temperatures. Dust input into the interstellar medium by AGB stars consists mostly of carbonaceous dust, with little SiC or silicate dust. Only the two coolest stars show a 30-μm band due to MgS dust. We suggest that this is due to the fact that, in the SMC, mass-losing AGB stars generally have low circumstellar (dust) optical depth and therefore effective heating of dust by the central star does not allow temperatures below the 650 K necessary for MgS to exist as a solid. Gas phase C_2H_2 bands are stronger in the SMC than in the LMC or Galaxy. This is attributed to an increasing C/O ratio at low metallicity. We present a colour–colour diagram based on *Spitzer* InfraRed Array Camera (IRAC) and Multiband Imaging Photometer for *Spitzer* (MIPS) colours to discriminate between O- and C-rich stars. We show that AGB stars in the SMC become carbon stars early in the thermal-pulsing AGB evolution, and remain optically visible for $\sim 6 \times 10^5$ yr. For the LMC, this lifetime is $\sim 3 \times 10^5$ yr. The superwind phase traced with *Spitzer* lasts for $\sim 10^4$ yr. *Spitzer* spectra of a K supergiant and a compact H II region are also given.

Key words: stars: AGB and post-AGB – stars: carbon – circumstellar matter – stars: mass-loss – Magellanic Clouds – infrared: stars.

1 INTRODUCTION

The late stages of the evolution of low- and intermediate-mass stars (hereinafter LIMS) are characterized by intense mass loss. This mass loss during the asymptotic giant branch (AGB) phase leads to the formation of a circumstellar envelope composed of gas and dust. The chemical composition depends strongly on the C/O abundance ratio. CO is one of the first molecules to form and is very stable and unreactive. If C/O > 1 by number, O will be trapped in the CO molecules, leading to a chemistry dominated by molecules such as C_2, C_2H_2, HCN and SiC dust grains (carbon stars). On the other

⋆E-mail: eric.lagadec@manchester.ac.uk

hand, if C/O < 1 we will observe oxygen-rich stars showing SiO, OH, H_2O molecules and silicate dust.

The study of this mass loss is of high astrophysical interest, and impacts on the chemical evolution of galaxies. Indeed, the mass loss from LIMS contributes to roughly half of all the gas recycled by stars (Maeder 1992). Mass loss from LIMS is one of two main sources (along with WR stars and supernovae associated with massive stars) of carbon in the universe (Dray et al. 2003). LIMS are also the main source of heavy s-process elements (e.g. Ba, Pb) and, when including post-AGB evolution (e.g. novae), the major stellar source of lithium.

The mass-loss process is, however, not fully understood. The mass loss results from a complicated interplay between stellar processes (turbulent convection, pulsation) and circumstellar processes (pulsation-driven shocks, radiation pressure) where especially the role of the dust composition is disputed (Woitke 2006). The effect of metallicity on the mass-loss rates is poorly understood and may vary with dust chemistry. Observational studies show no difference between peak gas mass-loss rates for Large Magellanic Cloud (LMC) and Small Magellanic Cloud (SMC) stars (e.g. van Loon 2006). Theoretical studies (e.g. Bowen & Willson 1991) predict that the mass-loss rates in AGB stars depend on the metallicity: a lower metallicity leads to a lower dust-to-gas ratio and less efficient dust-radiation pressure. The effect may also depend on the dust composition. In O-rich stars, dust is mostly composed of silicates and oxides, whilst in C-rich stars amorphous carbon, soot and SiC are observed. In O-rich stars, all dust species depend on heavy elements such as Si and Mg. In C-stars, dust can form from organic molecules which are affected differently by metallicity.

The sensitivity reached by the *Spitzer Space Telescope* (Werner et al. 2004) enables, for the first time, the determination of mass-loss rates from stars of different masses all along the AGB sequence at the distance of the Magellanic Clouds. The distances to these two galaxies are also relatively well known and the metal abundance of stars within can be estimated using age–metallicity relations. This allows one to measure absolute (dust) mass-loss rates for stars with known bolometric magnitudes and metallicities.

We have therefore conducted a survey of mass-losing stars in the SMC and LMC. The aim of this project is to empirically calibrate the mass-loss rate of AGB stars as a function of mass, luminosity and metallicity. Here we present the data from the SMC. The data from the LMC are presented in Zijlstra et al. (2006). A study of the mass-loss rates will be presented in forthcoming papers.

2 TARGET SELECTION

We selected 17 stars in the SMC to obtain a sample of stars of lower metallicity than the LMC stars described in Zijlstra et al. (2006). The stars were all AGB stars, with preference being given to stars in the populous intermediate-age cluster NGC 419, stars with past infrared (IR) monitoring showing large-amplitude variability or stars with some *ISO* (*Infrared Space Observatory*) detection (Cioni et al. 2003).

The observed stars are shown in the M_K versus $J-K$ diagram in Fig. 1. 14 of the intended targets were observed with *Spitzer*, while peak-up failures occurred for three objects. In one case, the peak-up occurred on a noise spike so no target was observed, while in the other two cases a brighter object in the peak-up image led to the detection of an H II region (MB 88, from Murphy & Bessell 2000) and a red supergiant of spectral type K (PMMR 52, from Prévot et al. 1983). The latter object is the single object lying in the supergiant region of Fig. 1.

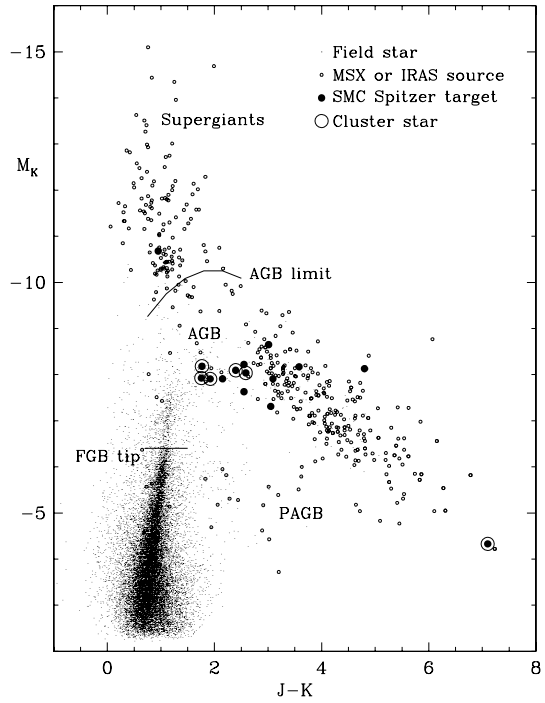

Figure 1. The M_K, $J-K$ diagram for the observed sample of mid-IR sources in the SMC (large filled circles). Stars in the cluster NGC 419 are circled. For orientation, we also show a large sample of mid-IR sources in the LMC from MSX (small open circles) and field stars from a small area of the LMC bar (small dots) – see also Zijlstra et al. (2006). AGB stars are confined approximately to the region below the line marked 'AGB limit'. Stars above this limit are red supergiants with masses above $\sim 8\,M_\odot$, or perhaps foreground stars. Distance moduli of 18.54 and 18.93 have been assumed for the LMC and SMC, respectively (Keller & Wood 2006).

The observed stars in the cluster NGC 419 whose names contain LE (NGC 419 LE 16, NGC 419 LE 18, NGC 419 LE 27 and NGC 419 LE 35) were discovered by Lloyd Evans (1980) using photographic surveys in the *V* and *I* bands. The two other stars from this cluster, NGC 419 IR 1 and NGC 419 MIR 1 were discovered during a survey with *Infrared Space Observatory* camera (ISOCAM) (Tanabe et al. 1997). LEGC 105 was discovered during an optical survey of the SMC (Lloyd Evans, Glass & Catchpole 1988). RAW 960 appeared in the Rebeirot, Azzopardi & Westerlund (1993) catalogue. IRAS 00554−7351 is described in Whitelock et al. (1989). Stars with names beginning with *ISO* were selected from the *ISO*/MACHO catalogue of variable AGB stars in the SMC (Cioni et al. 2003). The variable star GM 780 was discovered by Glen Moore using UK Schmidt plates but his work is unpublished. Literature data are summarized in Table 1. For LEGC 105, Lloyd Evans et al. (1988) suspect that the pulsation is irregular but their approximate period is confirmed with MACHO. RAW 960 has a very short period and is clearly a semiregular rather than a Mira variable.

All 14 AGB stars that were observed turned out to be carbon stars. The dominance of C stars is at variance with the Midcourse Space Experiment (MSX) based classification scheme of Egan, Van Dyk & Price (2001) according to which the sample stars would be a mixture of carbon-rich and oxygen-rich stars. Our LMC sample of AGB stars also showed that the Egan et al. classification scheme is ineffective at separating M and C stars on the AGB (Zijlstra et al. 2006).

Table 1. Bolometric magnitudes and periods from the literature. B83: Bessell, Wood & Evans (1983); W91: Westerlund et al. (1991); T97: Tanabe et al. (1997); vL05: van Loon et al. (2005); W89: Whitelock et al. (1989); LE88: Lloyd Evans et al. (1988); C03: Cioni & Habing (2003). The distance modulus to the SMC is taken as 18.93.

Star	$M_{\rm bol}$ (mag)	Period (d)	Ref.
NGC 419 LE 27	−4.88, −4.98		B83, W91
NGC 419 LE 18	−4.72, −4.82		B83, W91
NGC 419 LE 16	−5.43		W91
NGC 419 LE 35	−5.02		W91
NGC 419 IR 1	−4.9, −5.3		T97, vL05
NGC 419 MIR 1	−4.9		vL05
IRAS 00554−7351	−6.1	800	W89
LEGC 105	−4.7	310, 350	LE88, C03
RAW 960		34	C03
ISO 00573	−5.3	348	C03
ISO 01019	−5.1	336	C03
ISO 00548	−4.9	432	C03
ISO 00549	−5.6	604	C03

The AGB stars in our SMC sample have *JHK* colours which are reddened compared to stellar colours, but mostly not extremely so. The $J-K$ versus M_K diagram is shown in Fig. 1. The SMC sample has predominantly lower circumstellar extinction (bluer $J-K$ colours) than the LMC sample in Zijlstra et al. (2006). The cluster stars from NGC 419 are mostly at the blue end of the AGB sequence, but they also include the reddest star in the sample (NGC 419 MIR 1). IRAS 00554−7351 is also very red with $J-K=5$.

Fig. 2 shows the colour–magnitude diagrams for known optical carbon stars in the clouds. Open circles show the *Spitzer* samples of Zijlstra et al. (2006) and this paper. The distribution shows that we are observing the peak of the luminosity range of the optical carbon star distribution. The LMC sample contains a larger fraction of redder objects with higher dust mass-loss rates than the SMC sample. The gas mass-loss rates may be more compatible (e.g. Matsuura et al. 2006; van Loon 2006). However, this point should be taken into account when comparing the samples, as later in this paper.

3 OBSERVATIONS

3.1 *Spitzer*

The observations were made with the InfraRed Spectrograph (IRS; Houck et al. 2004), on board the *Spitzer Space Telescope*. We used the short-low (SL) and long-low (LL) modules to cover the wavelength range 5–38 μm. The SL and LL modules are each divided in two spectral segments, together known as SL2, SL1, LL2 and LL1; a 'bonus' order covering the overlap between the two modules is also available. The data reduction is similar to that described in Zijlstra et al. (2006). The raw spectra were processed through the *Spitzer* pipeline S12. We replaced the bad pixels by values estimated from neighbouring pixels. The sky subtraction was done by differencing images aperture-by-aperture in SL and nod-by-nod in LL. We used the software SPICE (*Spitzer* IRS Custom Extractor) to extract the spectra. The flux calibration was made using the reference stars HR 6348 (K0 III) in SL and HR 6348, HD 166780 (K4 III) and HD 173511 (K5 III) in LL. The spectra were individually extracted from the individual images. Both nods in both apertures were then joined simultaneously, recalculating the errors in the process by comparing the nods. The different nods were averaged, using the differences to estimate the errors. The different spectral segments were combined using scalar multiplication to eliminate the discontinuities due to flux lost because of pointing errors. The different segments were also trimmed to remove dubious data at their edges. We also retained the bonus order where it was valid. We obtained a standard wavelength calibration accuracy of 0.06 μm in SL and 0.15 μm in LL. The calibration process is detailed in Sloan, Neremberg & Russel (2003).

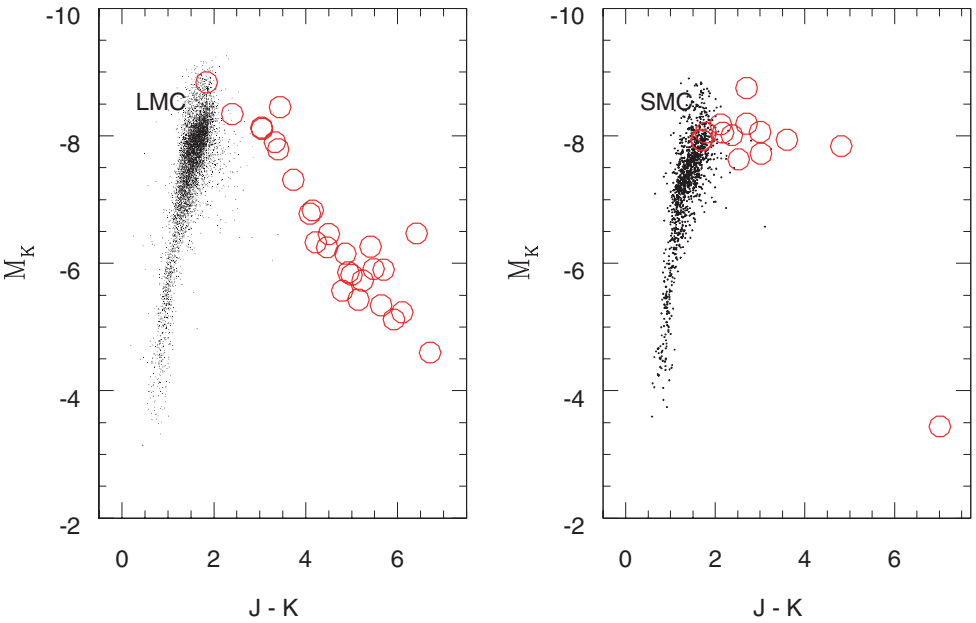

Figure 2. The M_K, $J-K$ diagram for all known optical carbon stars in the LMC and SMC. Samples are taken from Rebeirot et al. (1993) and Kontizas et al. (2001); IR magnitudes are from 2MASS. Open circles show the *Spitzer* targets discussed in Zijlstra et al. (2006) and in this paper. LMC photometry for these is from Groenewegen et al. (in preparation), where no J is available, we assumed $J-K\sim0.6+1.84\times(H-K)$. The $J-K\approx7$ for NGC 418 MIR 1 was estimated from its $K-L$ colour.

Even after sky removal, some interstellar emission lines remain on the spectra, mostly observed longward of 30 μm.

Two of the observed objects in NGC 419, LE 35 and LE 27 showed large discrepancies between SL and LL. The apertures of these two modules are perpendicular to each other on the sky. An acquisition error may have led to the star being missed in one aperture but not the other, or confusion in the cluster may have caused spectrum extraction problems. The SL spectra are those of AGB stars, with flux densities consistent with the MSX flux. The LL spectra are too faint and featureless. We therefore consider the SL observations to have been successful and will only discuss their SL spectra. However, mispointings can affect the wavelength calibration, flux calibration and even the slope of the spectral energy distribution (SED). We can therefore not be as confident of these spectra as we are for the remaining stars.

The spectra of the observed AGB stars, ordered by dust temperatures (see Section 6), are presented in Fig. 3. The molecular bands discussed below show that all 14 objects are carbon-rich stars. We calculated equivalent magnitudes of our sources for InfraRed Array Camera (IRAC) 8 μm and Multiband Imaging Photometer for *Spitzer* (MIPS) 24 μm, by convolving these filter band passes with our spectra. These are listed in Table 2.

Finally, we present the spectra of the two objects acquired accidentally following peak-up failure. MB 88 (Fig. 4) is a red object with emission lines, a spatial diameter of about 8 arcsec, and with several embedded stars. It is almost certainly an H II region. Emission lines from S IV (10.51 μm), Ne II (12.81 μm), S III (18.71 and 33.48 μm), Si II (34.83 μm) and Ne III (35.97 μm) are observed. Its spectrum is not analysed further here. The spectrum of the red supergiant PMMR 52 can be found in Fig. 5. It is discussed briefly in Section 5.1.

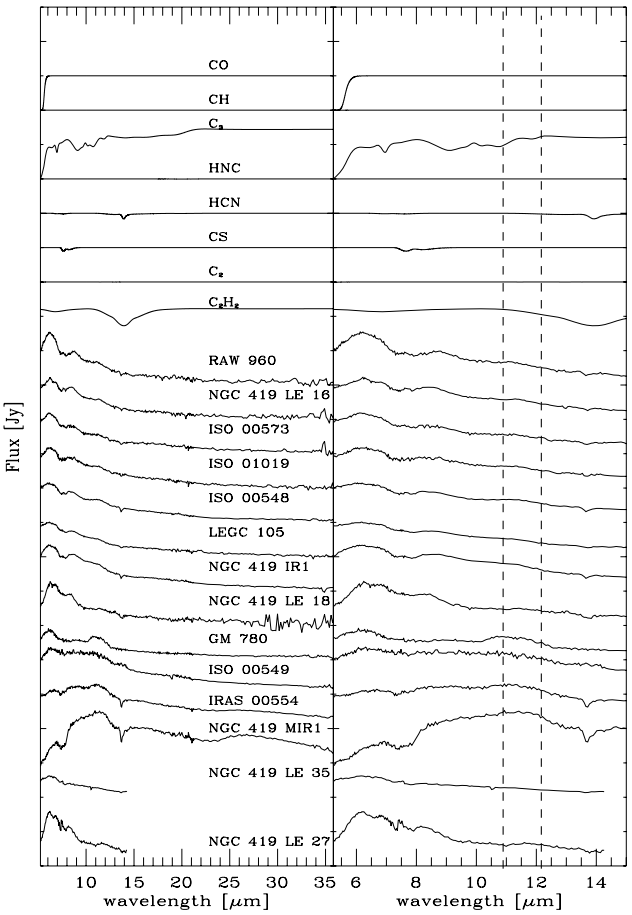

Figure 3. Spectra of the carbon-rich stars observed in the SMC. The two stars at the bottom have been observed only in SL. All other stars are ordered by dust temperature. Blue stars are at the top and red ones at the bottom. Molecular templates are shown at the top (see Section 4.3). The dashed lines show the location of the SiC feature.

3.2 Bolometric magnitudes and initial masses

We determined the bolometric magnitudes of the observed stars assuming a SMC distance modulus of 18.93 ± 0.024 (Keller & Wood 2006) (∼60 kpc). *JHKL* photometry was taken nearly simultaneously with the *Spitzer* observations. These observations were made using the 2.3-m telescope at Siding Spring Observatory (SSO, Australia). The filters used were centred at 1.28 μm (*J*), 1.68 μm (*H*), 2.22 μm (*K*) and 3.59 μm (*L*). The observations are described in Groenewegen et al. (2007). Zero flux was assumed at the frequencies 0 and 3×10^{16} Hz to estimate the bolometric magnitudes. The flux from the star was then estimated by integrating under the resulting SED. The line-of-sight extinction towards the SMC of $E(B-V) = 0.12$ (Keller & Wood 2006) was ignored. The bolometric magnitudes are presented in Table 2.

Simultaneous observations in the *K*-band are important to obtain a reliable instantaneous luminosity estimate. However, the magnitudes are single-epoch measurements and therefore subject to pulsation-induced variability. Earlier (literature) values are listed in Table 1. These generally agree to within 0.5 mag of the current measurements, consistent with the variability expected for these stars.

The histogram of the distribution is shown in Fig. 6. The SMC sample includes the carbon stars observed by Sloan et al. (2006) which cover a similar luminosity range. The LMC carbon-star sample of Zijlstra et al. (2006) is also shown. There is no obvious difference between the LMC and SMC distributions.

For comparison, in the third panel we show a complete carbon star luminosity function for the LMC. This is derived from the carbon star survey of Kontizas et al. (2001), which we cross-correlated with Two Micron All Sky Survey (2MASS). The bolometric magnitudes for this sample are derived from the 2MASS *JHK* magnitudes, using the bolometric correction equation derived by Whitelock et al. (2006):

$$\mathrm{BC}_K = +0.972 + 2.9292\,(J-K) - 1.1144\,(J-K)^2 + 0.1595\,(J-K)^3 - 9.5689 \times 10^3 (J-K)^4. \quad (1)$$

This relation differs by 0.2–0.3 mag from the one used by Costa & Frogel (1996) for $1 < J-K < 2.5$. Positional agreement between the 2MASS object and the carbon star is required to be better than 1 arcsec. Stars with non-detections in one or more IR band are not included.

The bottom panel shows the same for the SMC carbon stars taken from Rebeirot et al. (1993). These stars were also cross-correlated with 2MASS, and the bolometric magnitudes derived from the 2MASS *JHK* magnitudes. The coordinates in Rebeirot et al. are less accurate and we accepted co-identifications out to 2 arcsec. A larger number of chance superpositions may be expected.

If we compare this histogram with fig. 20 in Vassiliadis & Wood (1993), for SMC metallicities, this indicates that the stars we observed have initial masses in the range 1–4 $\mathrm{M}_\odot$.

Six of the stars we observed are located in the cluster NGC 419. This cluster has an age of 1.2×10^9 yr, and a metallicity [Fe/H] =

Table 2. Observed SMC targets: names, adopted coordinates and photometry. *J* and *K* are taken from near-simultaneous measurements at SSO. The 8 and 24 μm magnitude are calculated from our spectra using the IRAC and MIPS filter profiles; the zero-points are taken as 63.5 Jy (8.0 μm) and 7.14 Jy (24 μm), respectively.

Adopted name	2MASS name	RA	Dec. (J2000)	*J* (mag)	*K* (mag)	8 μm (mag)	24 μm (mag)	m_{bol} (mag)	M_{bol} (mag)
AGB stars									
NGC 419 LE 27	01082067−7252519	01 08 20.67	−72 52 52.0	12.68	10.99	6.05		14.49	−4.44
NGC 419 LE 18	01082495−7252569	01 08 24.95	−72 52 56.9	12.71	11.00	9.09	8.76	14.43	−4.50
NGC 419 LE 35	01081749−7253013	01 08 17.49	−72 53 01.3	12.67	10.88	7.16		14.33	−4.60
NGC 419 LE 16	01080114−7253173	01 08 01.14	−72 53 17.4	13.82	11.30	8.72		14.65	−4.28
NGC 419 IR 1	01081296−7252439	01 08 12.97	−72 52 44.0	13.44	10.74	7.31	6.79	13.71	−5.22
NGC 419 MIR 1		01 08 17.47	−72 53 09.5		15.49			14.33	−4.60
IRAS 00554−7351	00570395−7335146	00 57 03.95	−73 35 14.7	15.90	11.09	5.69	4.12	12.67	−6.26
RAW 960	00555464−7311362	00 55 54.65	−73 11 36.3	13.29	10.92			14.42	−4.51
ISO 00573	00572054−7312460	00 57 20.55	−73 12 46.0	12.87	10.75	8.61	8.20	14.17	−4.76
LEGC 105	00544685−7313376	00 54 46.85	−73 13 37.7	14.23	11.21	8.18	7.85	14.36	−4.57
ISO 01019	01015458−7258223	01 01 54.58	−72 58 22.4	13.05	10.88	8.21	8.12	14.15	−4.78
ISO 00548	00545075−7306073	00 54 50.76	−73 06 07.4	13.87	10.87	7.45	7.12	13.84	−5.09
ISO 00549	00545410−7303181	00 54 54.11	−73 03 18.2	14.59	10.99	7.24	6.14	13.80	−5.13
GM 780	00353726−7309561	00 35 37.27	−73 09 56.2	12.88	10.18	7.67	6.57	13.58	−5.35
Other objects									
PMMR 52		00 53 09.12	−73 04 03.8						
MB 88		00 51 40.4	−73 13 33						

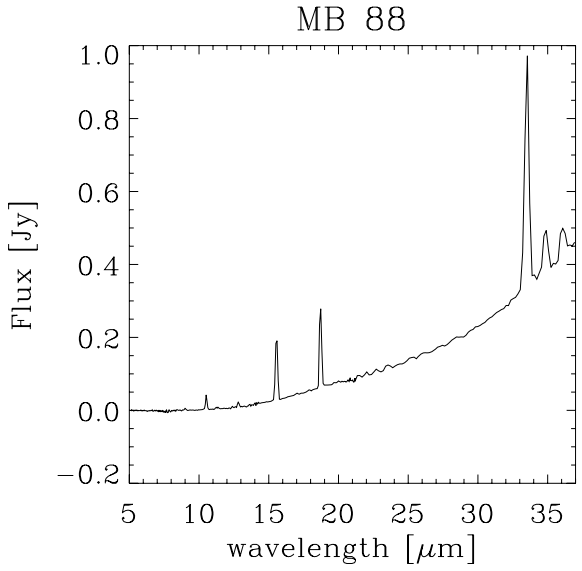

Figure 4. Spectrum of the red object MB 88. This object shows emission lines and could be associated with an H II region. Emission lines from S IV (10.51 μm), Ne II (12.81 μm), S III (18.71 and 33.48 μm), Si II (34.83 μm) and Ne III (35.97 μm) are observed.

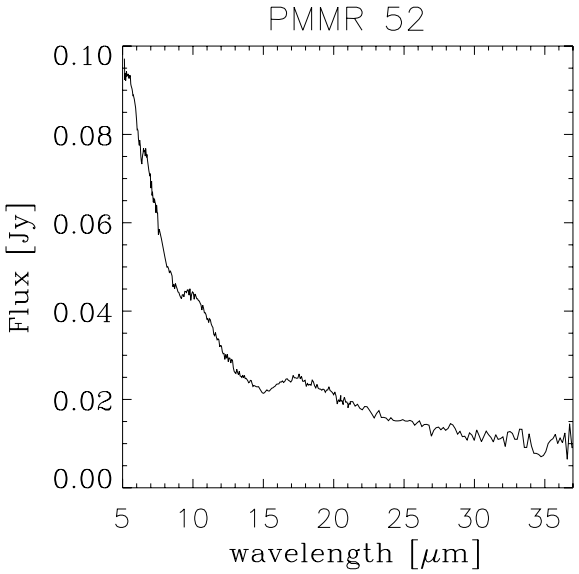

Figure 5. Spectrum of the oxygen-rich star PMMR 52. Typical spectral features of silicates are observed at 9.8 and 18 μm.

−0.60 ± 0.21 (de Freitas Pacheco, Barbuy & Idiart 1998). The isochrones of Pietrinferni et al. (2006) for this age and for $Z = 0.004$ give an initial mass of the thermal-pulsing AGB stars in this cluster of 1.82 $M_\odot$ for standard models and 2.08 $M_\odot$ for models using overshoot. (The difference shows the considerable uncertainty in deriving stellar ages.) However, their bolometric magnitudes (see also van Loon, Marshall & Zijlstra 2005) are associated with higher mass progenitors on the Vassiliadis & Wood (1993) tracks. Thus the stars reach a higher luminosity than predicted. This may indicate that the mass loss is weaker (or the onset of the superwind later) than assumed for the evolutionary model calculations (Zijlstra 2004). This could also been explained by a later onset of greatly enhanced mass loss, the superwind phase necessary to explain the densities seen in typical planetary nebulae (Renzini 1981). (Zijlstra et al. 2006 define the superwind as the phase where the mass-loss rate exceeds the nuclear burning rate.)

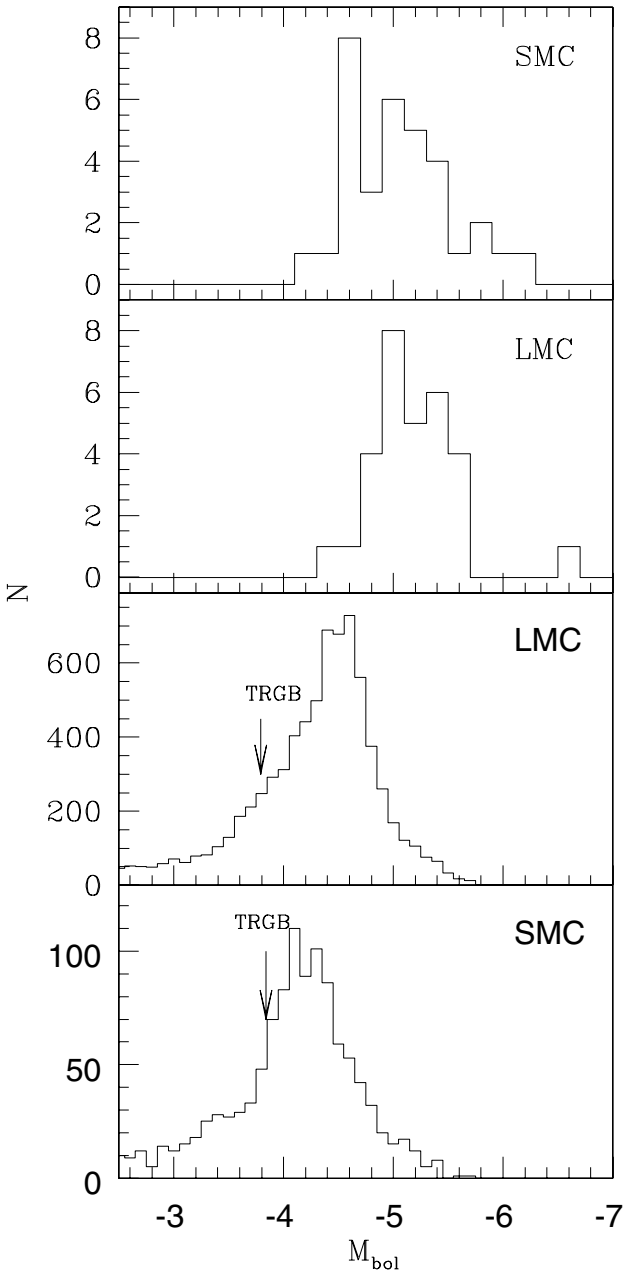

Figure 6. Top: distribution of bolometric magnitudes of the observed stars in the SMC, assuming a distance modulus of 18.93 (Keller & Wood 2006). Both stars from this paper and from Sloan et al. (2006) are included. Second: the histogram for the LMC carbon stars observed by *Spitzer* (Zijlstra et al. 2006). Third: optical carbon stars in the LMC (Kontizas et al. 2001). Bottom panel: optical carbon stars in the SMC (Rebeirot et al. 1993). The arrows indicate the location of the tip of the red giant branch (RGB) (Bellazzini, Ferraro & Pancino 2001).

4 OBSERVED SPECTRAL FEATURES

The spectra show clear and deep molecular bands. The two main dust features are less obvious. We will describe the dust bands first, followed by the observed molecular bands.

4.1 Dust bands

Most of the carbon stars in our sample show the presence of an emission feature around 11.3 μm. This feature is attributed to emission from SiC. However, in several cases the feature is very weak, and in such cases it is hard to judge whether this feature is an emission feature or due to molecular absorptions on the blue and red side. SiC condenses at high temperatures and is expected to be present for all dusty carbon stars. However, its abundance may be limited by the abundance of Si.

NGC 419 LE 35 shows no discernable SiC feature. This is, however, one of the two sources with acquisition and/or extraction problems. GM 780 has a very strong feature, compared to the other stars, but the shape is peculiar. The shape is possibly affected by extraction problems but the strength of the feature is well established. This object is discussed below.

A wide emission feature, centred at ∼30 μm is observed in two stars: NGC 419 MIR 1 and (weaker) IRAS 00554−7351. This feature is common in Galactic AGB and post-AGB stars, and attributed to emission from MgS (Hony, Waters & Tielens 2002). These two SMC stars have the reddest near-IR colours in our sample, and the coolest dust, with dust temperatures of, respectively, 409 and 589 K (see Section 6). In the LMC, this feature is observed only in the envelopes of stars with dust temperature lower than 650 K (Zijlstra et al. 2006). This can be explained by the fact that MgS grows on the surface of pre-existing grains, this process starting around 600 K and being complete around 300 K. The two SMC detections are consistent with this.

4.2 Molecular bands

Most vibrational bands of simple molecules occur at wavelengths shortward of 20 μm. (HNC has a vibrational fundamental at 20 μm.) This is the region where we observe clear bands. The main features, observed for most of the stars of our sample, are located at ∼7.5 and ∼13.7 μm, respectively. Both are associated with absorption from C_2H_2. The 13.7-μm band is due to the ν_5 bending mode of acetylene and its associated hot and combination bands (Cernicharo et al. 1999). This absorption band is observed in almost all carbon stars of our sample, but it is not clear in ISO 00549 and GM 780. The narrow band is flanked by broader bands, best seen in NGC 419 MIR 1. The double peaked band at 7.5 μm observed in all of our spectra is associated with the C_2H_2 $\nu_4^1 + \nu_5^1$ P- and R-branch transition, as shown by Matsuura et al. (2006). The shape may be different in NGC 19 LE 27, perhaps with a contribution from CS and/or HCN.

A weak absorption band at 14.3 μm is observed in the spectra of the two reddest stars of our sample (IRAS 00554 and NGC 419 MIR 1). This band has been observed in Galactic carbon stars (Aoki, Tsuji & Ohnaka 1999) and is attributed to HCN. The fact that it is observed in the reddest stars of our sample, where the optical depth is important, and dust coolest seems to indicate that this molecule is present in the outer layers of the observed envelopes. This is corroborated by the fact that this molecule is also observed in a LMC star where the continuum temperature and optical depth are such that the photosphere cannot be seen (Speck et al. 2006).

A decrease of the SED is observed near the blue edge of all our spectra, around 5 μm. This is due to several molecules: C_2 and/or C_3 starting from 6 μm (blueward), and CO absorption very close to the 5 μm. Several targets show a higher flux level at the blue edge with a sharp drop: this is not seen in the LMC spectra.

Zijlstra et al. (2006) have identified a weak absorption feature in the LMC sample at 5.8 μm, attributed to carbonyl. This feature is not detected in our SMC sample. It could indicate an underabundance of CO with respect to stars in the LMC, as expected given that there is less O to start with.

4.3 Models of molecular opacity

The top lines in Fig. 3 show the calculated model spectra of a number of molecules. Similar plots in Zijlstra et al. (2006) are based on the line lists and models of Jørgensen, Hron & Loidl (2000). Newer line lists are now available for some simple molecules (Harris, Polyansky & Tennyson 2002; Harris et al. 2006), such as HCN and HNC. We also revised opacity curves for CO, C_2 and CS from Zijlstra et al. (2006).

The HCN/HNC line list was computed using first principles quantum mechanics. It contains about 160 000 rotation-vibration energy levels truncated at 18 000 cm^{-1}, and at $J = 60$. There are around 4×10^8 lines, but only 34×10^6 of these are strong enough to contribute to opacity. Both the linear H-CN and H-NC geometric configurations are studied, as are some of the low lying delocalized states. The delocalized states are the states in which the H nucleus orbits the CN part of the molecule. The accuracy of the fundamental vibrational transitions is about 3–4 cm^{-1}; the error increases at higher energies. The transition intensities agree well with laboratory data. Incorporation of laboratory data into the line list has significantly improved the accuracy of the frequencies of the transitions between these low lying states.

The opacity curves for CO, C_2 and CS are calculated from absorption coefficients determined by Querci et al. (1971), Goorvitch (1994) and Chandra et al. (1995), respectively.

Using this, we determined the opacity for the HCN, HNC, CO, CS and C_2 as a function of wavelength. To determine the transmission function, we then used the Lambert–Beer law (Banwell & McCash 1994), i.e. the solution to the one-dimensional (1D) equation of radiative transfer in the absence of an internal source.

Fitting the spectral features to get column densities is beyond the scope of this paper and will be done in a forthcoming paper. We can however determine which molecules are responsible for the observed molecular bands. We thus calculated transmission curves using column densities for the different molecular species of 10^{18} cm^{-2} for the HCN, HNC, CS and C_2 molecules and 10^{22} cm^{-2} for CO. A temperature of 1750 K was used for all the models. The resulting transmittance curves are plotted at the top of Fig. 3, together with the transmittance curves from Jørgensen et al. (2000) for C_2H_2 and C_3. This C_2H_2 model reproduces the broad photospheric absorption, but not the narrow component, arising from a cool layer (Jørgensen et al. 2000). Cherchneff (2006) shows that acetylene reaches its peak abundance in the extended atmosphere, and its temperature is expected to be lower than the photospheric temperature (Matsuura et al. 2006; van Loon et al. 2006).

5 INDIVIDUAL STARS

5.1 PMMR 52

PMMR 52 is a red supergiant of spectral type K (Prévot et al. 1983). This is the only oxygen-rich star in the sample. The spectrum is shown in Fig. 5. The observed spectrum of PMMR 52 shows the presence of spectral features of oxygen-rich dust (silicates at 10 and 18 μm). The 18-μm silicate feature is strong. The 10-μm silicate band is remarkably weaker than observed in other O-rich stars. Normally, in O-rich stars, the 18-μm feature should decrease steeply after 19–20 μm. However, the one in PMMR 52 remains very flat.

There are no signatures of crystalline silicates, which indicate that the silicates are largely in an amorphous phase. Some small absorption features are observed at 6.2 and 7.5 μm. The 6.2-μm feature is due to water, while the one at 7.5 μm might be attributed to absorption by SiO, but this feature is very faint and might be due to noise.

5.2 GM 780

Fig. 7 shows the spectrum of GM 780. Compared to the other sources, C_2H_2 bands are noticeably absent. The weak band at 8 μm is best fitted as CS, based on the models above. The 11-μm band is strong but its shape is significantly different from that of the other stars. There are no traces of silicates at 9.8 and 18 μm. GM 780 is the brightest star at K in our sample; the bolometric luminosity is high for our sample but lower than those of the luminous IRAS-selected carbon stars (van Loon, Zijlstra & Groenewegen 1999a).

The $J - K$ colour of this object, $J - K = 2.6$, is quite red, and dust should be present around it. The dust temperature is relatively high, however, at 720 K.

The object is discussed further below (Section 9) where we argue that this star has a C/O ratio lower than that of other stars in the sample.

6 COLOURS AND BAND STRENGTHS

As discussed above, the spectra of the observed stars are dominated by molecular and dust bands. This makes the definition of the continua difficult. To avoid this and to determine colours, we use the Manchester system (Sloan et al. 2006; Zijlstra et al. 2006). This system, valid for carbon stars but not for oxygen-rich stars, defines four narrow bands, selected to avoid the molecular and dust bands, to determine the continuum. Table 3 shows the wavelengths used to define the four narrow bands and the adopted flux corresponding to zero magnitude, determined to give a zero colour for a Rayleigh–Jeans tail. Using this system, we can determine continuum flux at 6.4, 9.3, 16.5 and 21.5 μm by integrating the observed spectra over the defined bands. The choice of the wavelengths used to define the continua is discussed in Zijlstra et al. (2006). Table 4 lists the measured continuum flux and colours for the observed carbon stars.

This method permits us to determine two colour temperatures, [6.4]–[9.3] and [16.5]–[21.5]. The [6.4]–[9.3] colour is an indication of the optical depth, whereas the [16.5]–[21.5] colour can be use to determine the dust temperature. Table 6 lists the blackbody temperatures derived from the [16.5]–[21.5] colours for the observed stars. For the bluest objects, this method gives lower limits ($\lesssim 10^4$ K) as the Rayleigh–Jeans limit is reached. This is the case for NGC 419 LE 16, NGC 419 IR 1, RAW 960, LEGC 105, ISO 00573, ISO 01019 and ISO 00548. We thus do not give an estimation of the dust temperature for these stars. Furthermore, the derived temperature can be affected by wavelength-dependent continuum contamination from other sources in the beam. Thus, for the bluest stars, we can obtain temperatures that are not physically meaningful.

Fig. 8 shows the [6.4]–[9.3] versus [16.5]–[21.5] colour–colour diagram obtained with the Manchester method. The stars from our

Table 3. Mid-IR continuum bands for carbon stars for the so-called 'Manchester system'. The last column gives the adopted flux corresponding to zero magnitude.

Central λ (μm)	λ range (μm)	F_0 (Jy)
6.4	6.25–6.55	96.5
9.3	9.1–9.5	45.7
16.5	16–17	15.4
21.5	21–22	9.1

Table 4. Photometry: colours measured using four narrow carbon stars continuum bands.

Target	[6.4]–[9.3] (mag)	[16.5]–[21.5] (mag)
NGC 419 LE 27	0.067 ± 0.018	
NGC 419 LE 18	0.067 ± 0.020	0.126 ± 0.098
NGC 419 LE 35	0.215 ± 0.013	
NGC 419 LE 16	0.325 ± 0.021	−0.052 ± 0.062
NGC 419 IR 1	0.496 ± 0.011	0.047 ± 0.017
NGC 419 MIR 1	1.343 ± 0.012	0.352 ± 0.012
IRAS 00554	0.938 ± 0.008	0.232 ± 0.021
RAW 960	0.199 ± 0.022	0.017 ± 0.115
ISO 00573	0.255 ± 0.017	−0.012 ± 0.029
LEGC 105	0.380 ± 0.013	0.034 ± 0.069
ISO 01019	0.374 ± 0.015	−0.156 ± 0.039
ISO 00548	0.399 ± 0.013	−0.084 ± 0.025
ISO 00549	0.725 ± 0.014	0.199 ± 0.012
GM 780	0.388 ± 0.016	0.185 ± 0.031

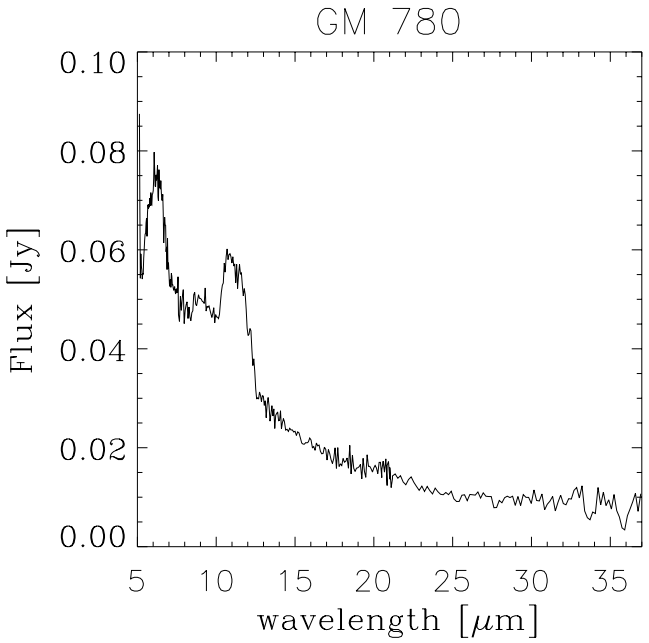

Figure 7. The peculiar spectrum of GM 780.

sample form a well-defined sequence on this diagram. Some stars show a negative [16.5]–[21.5] colour (NGC 419 LE 16, ISO 00573, ISO 01019, ISO 00548). These stars are very blue and their spectra are typical of naked carbon stars. Two blue stars, NGC 419 LE 18 and GM 780, are offset in [16.5]–[21.5] colour by roughly 0.1 mag. The spectrum of GM 780 is very noisy in LL, so that its [16.5]–[21.5] colour has higher uncertainties than the other objects. The good correlation observed between [6.4]–[9.3] and [16.5]–[21.5] indicates that the choice of our continuum wavelengths is appropriate.

For all the stars in our sample, we have measured the strength of the observed features. We define small wavelength ranges on the blue and red side of the features (Table 5), selected to avoid features, to define the continuum. We then fit line segments from both sides of the feature that defines the continuum. As the red edge of the MgS feature is outside of the IRS wavelength range, this method cannot be applied to the MgS feature. The continuum under the MgS feature is thus assumed to be a blackbody with a temperature deduced from the [16.5]–[21.5] colour. After subtraction of the continuum, we can measure the strength of each feature. For the molecular bands (C_2H_2 at 7.5 and 13.7 μm), this strength is estimated as an equivalent width. For the dust emission features (SiC and MgS), we use a line-to-continuum (L/C) ratio, defined as the integrated flux of the band divided by the integrated underlying continuum, over the wavelength range of the feature. The MgS feature extend beyond the edge of the spectral coverage: its strength relates only to the part blueward of 38 μm, and the continuum is calculated as a blackbody (see Zijlstra et al. 2006).

We also measured the central wavelength of the SiC band. This central wavelength is defined as the wavelength at which, after continuum removal, the flux on the blue side equals the flux on the red side. Table 6 lists the measured strength and central wavelengths of the observed features. The MgS feature central wavelength cannot be measured from the available wavelength range.

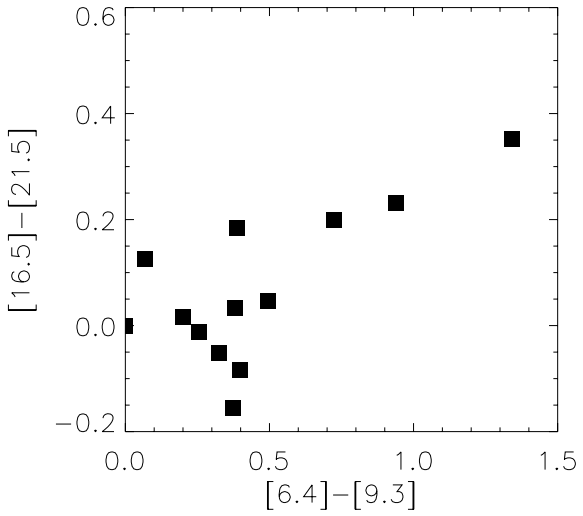

Figure 8. The [6.4]–[9.3] versus [16.5]–[21.5] colour–colour diagram of the stars in our SMC sample.

Table 5. Wavelengths used to estimate the continua for the SiC and C_2H_2 spectral features.

Features	λ (μm)	Blue continuum (μm)	Red continuum (μm)
C_2H_2	7.5	6.08–6.77	8.22–8.55
SiC	11.3	9.50–10.10	12.80–13.40
C_2H_2	13.7	12.80–13.40	14.10–14.70

7 COLOUR–COLOUR DISCRIMINATION BETWEEN C- AND O-RICH AGB STARS

Classification criteria for separating C-rich from O-rich stars proposed by Egan et al. (2001) are based on the $K - A$ versus $J - K$ colours (where A is the MSX band centred at 8.3 μm). These are now known not to work effectively (Buchanan et al. 2006; Zijlstra et al. 2006). Better separation is possible using different MSX bands (Whitelock et al. 2006) but in the Magellanic Clouds only the A band was sensitive enough to detect the AGB stars.

A variety of colour–colour plots based on IRAC and MIPS observations, useful in distinguishing chemical type, are discussed in

Table 6. Strength of the molecular and dust features, in terms of either the equivalent width in microns or the integrated L/C ratio (Section 6). The last column gives the continuum (blackbody) temperature, derived from the [16.5]–[21.5] colour listed in Table 4.

Target	EW (7.5 μm)	EW (13.7 μm)	L/C (SiC)	λ_c	L/C (MgS)	T (K)
NGC 419 LE 27	0.080 ± 0.015	0.057 ± 0.009	0.033 ± 0.009	11.96 ± 0.17		
NGC 419 LE 18	0.101 ± 0.009	0.151 ± 0.038	0.032 ± 0.016	11.46 ± 0.20		1038 ± 430
NGC 419 LE 35	0.129 ± 0.006	0.079 ± 0.006	−0.009 ± 0.004	10.48 ± 0.00		
NGC 419 LE 16	0.158 ± 0.011	0.033 ± 0.009	0.056 ± 0.009	11.33 ± 0.06		
NGC 419 IR 1	0.150 ± 0.002	0.044 ± 0.005	0.038 ± 0.004	11.05 ± 0.07		
NGC 419 MIR 1	0.187 ± 0.011	0.066 ± 0.005	0.101 ± 0.005	11.38 ± 0.05	0.392 ± 0.015	409 ± 12
IRAS 00554	0.102 ± 0.008	0.079 ± 0.004	0.119 ± 0.008	11.28 ± 0.08	0.276 ± 0.026	589 ± 44
RAW 960	0.230 ± 0.009	0.051 ± 0.010	0.057 ± 0.010	11.20 ± 0.11		
ISO 00573	0.148 ± 0.005	0.078 ± 0.013	0.056 ± 0.011	11.19 ± 0.18		
LEGC 105	0.116 ± 0.003	0.062 ± 0.006	0.019 ± 0.004	11.01 ± 0.11		
ISO 01019	0.151 ± 0.005	0.032 ± 0.013	0.033 ± 0.009	11.26 ± 0.13		
ISO 00548	0.138 ± 0.003	0.068 ± 0.002	0.068 ± 0.004	11.27 ± 0.04		
ISO 00549	0.047 ± 0.013	−0.041 ± 0.010	0.061 ± 0.012	11.21 ± 0.30		674 ± 34
GM 780	0.149 ± 0.010	0.006 ± 0.007	0.289 ± 0.011	11.13 ± 0.05		724 ± 94

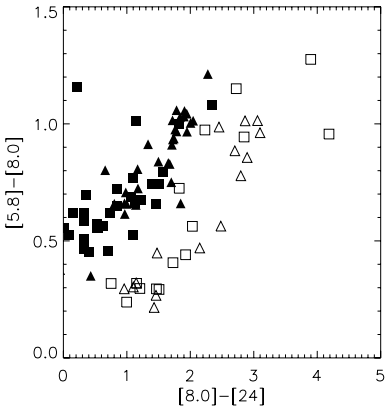

Figure 9. [8]–[24] versus [5.8]–[8.0] colour–colour diagram of AGB stars in the LMC and SMC. Black symbols represent AGB C-rich stars. Open symbols represent AGB O-rich stars. Squares correspond to stars in the SMC and triangles to stars in the LMC.

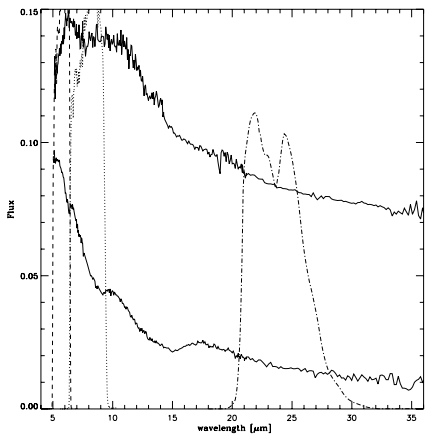

Figure 10. Spectra of two stars with the same [8]–[24] colours. No flux scaling has been applied. ISO 00549 (top) is a C-rich star. PMMR 52 (bottom) is an O-rich star. The transmission of the IRAC 5.8 μm (dashed line), 8 μm (dotted line) and MIPS 24 μm (dot–dashed line) filters are overlaid.

Blum et al. (2006). These, however, rely on the IRAC bands outside of the IRS wavelength coverage. We investigated whether a colour–colour diagram, based on *Spitzer* IRAC and MIPS colours, could discriminate O- and C-rich stars using $\lambda > 5$ μm. The equivalent IRAC and MIPS flux for the observed objects were derived from the IRS spectra and the transmission curves of the IRAC 5.8- and 8.0-μm filters and MIPS 24-μm filter. As our sample contains just one O-rich star, we added IRS spectra of evolved stars in the SMC and in the LMC from different programs.

Fig. 9 shows the distribution of the O-rich stars (open symbols) and C-rich stars (black symbols) from the combined sample on a [8.0]–[24] versus [5.8]–[8.0] colour–colour diagram. The O- and C-rich stars form two well-defined sequences on this diagram. The C-rich stars have redder [5.8]–[24] colour than O-rich stars for the same [8.0]–[24] colour. Fig. 10 explains this effect. We have plotted the spectra of PMMR 52, an O-rich star, and ISO 00549, a C-rich star, with the transmission of the IRAC 5.8 μm (dashed line), 8 μm (dotted line) and MIPS 24 μm (dotted–dashed line) bands superposed. The filter responses are affected by several molecular and dust bands. For O-rich stars, the blue edge of the MIPS 24-μm filter overlaps with the 18-μm silicate emission feature, and molecular absorption by SiO affects the 8-μm band. For carbon stars, the 5.8-μm band is suppressed by molecular absorptions. (We note that this IRAC band extends beyond the blue edge of our spectra.) A C-rich star with the same [8]–[24] colour as an O-rich star will have a continuum emission redder than the O-rich star. Such a diagram has been made by Buchanan et al. (2006) using their LMC sample containing redder stars.

Fig. 10 thus indicates that a [8]–[24] versus [5.8]–[8.0] diagram can be used to discriminate between C- and O-rich stars with colours within the range of the objects present in our sample ([8]–[24] < 4 and [5.8]–[8.0] < 1.4). Furthermore, the sample used in Fig. 9 contains stars in the LMC (triangles) and the SMC (squares). The SMC and LMC follow the same sequences, indicating that the difference of location of C- and O-rich stars in the colour–colour diagram is independent of metallicity.

8 AVERAGE SPECTRA FOR SMC AND LMC STARS

Fig. 11 shows the averaged spectra of the red SMC sources (top, solid line) and blue SMC sources (bottom, solid line), where 'red' and 'blue' are defined as in Zijlstra et al. (2006). To compare these

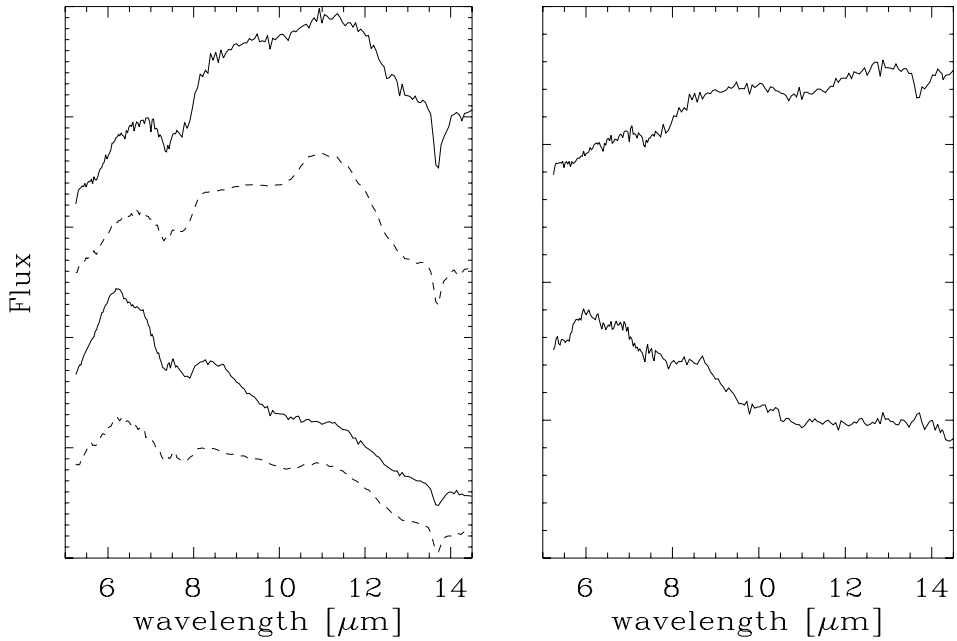

Figure 11. On the left, averaged spectra from our SMC sample (solid lines). The upper solid line shows the averaged spectrum of the red sources. The lower solid line shows the averaged spectrum of the blue sources. The dotted lines show the equivalent averaged spectra from the Zijlstra et al. LMC sample. The right-hand panel shows the SMC averaged spectrum divided by the LMC averaged spectrum for the red sources (top) and the blue sources (bottom).

spectra with LMC spectra, we overplot the LMC spectra on this figure (dotted lines). Those LMC spectra are taken from Zijlstra et al., and are, respectively, the spectra with weak SiC and no MgS in fig. 19 in that paper. The right-hand panel shows the ratio of the SMC averaged spectra and the LMC averaged spectra.

The LMC and the SMC spectra show the same features, but the differences are significant especially for the 'red' sources. The differences are associated with the C_2H_2 and the SiC bands. The fact that the acetylene features show as absorption in the ratio spectra indicates that these bands are relatively *stronger* in the SMC. The 13.7 μm is clearest seen, indicative of the colder circumstellar molecules. The 11.3-μm band also shows in absorption, but as this is an emission feature, the negative footprint here shows it to be *weaker* in the SMC.

The 'blue' sources do not show easily interpretable differences. The broad 10-μm absorption may contain a blue contribution from a molecular band (e.g. Zijlstra et al. 2006), in addition to SiC. The redward continuum may be affected by the photospheric broad 14-μm C_2H_2 band.

9 SILICON-CARBIDE DUST

9.1 Strength

Fig. 11 clearly indicates that the 11.3-μm SiC feature is stronger in the LMC than in the SMC, even if this feature is rather weak in blue sources. The divided spectra do not show any difference in the shape of the SiC feature in the SMC and the LMC, but only in the band strength. Thus, whereas the emission strength varies, the emission shape is constant. The composition of the SiC grains is likely the same for the two environments.

Fig. 12 shows the strength of the SiC feature as a function of the [6.4]–[9.3] colour. To study the effect of metallicity on the strength of the SiC features, we overlaid the measured strength of this feature

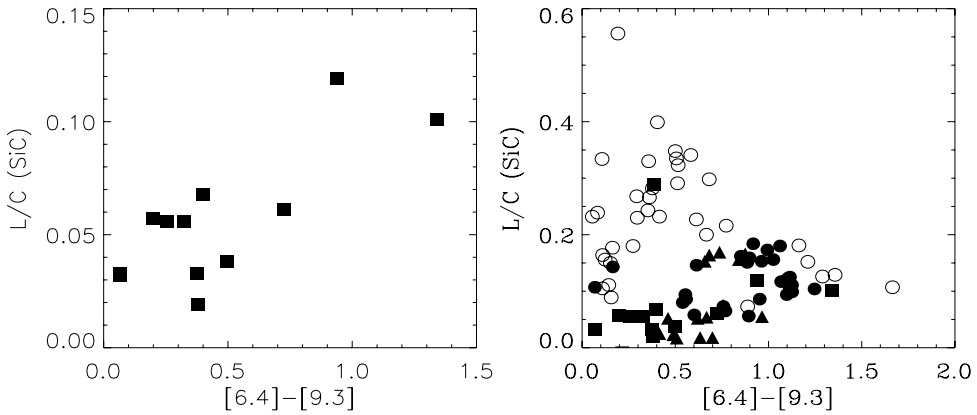

Figure 12. The strength of the SiC feature as a function of the [6.4]–[9.3] colour in our SMC sample (left-hand panel). The right-hand panel combines this with stars from Sloan et al. SMC and Galactic samples: filled squares represent our SMC sample, triangles represent Sloan et al. (SMC) sample, open circles represent Sloan et al. (Galactic) sample and filled circles represent Zijlstra et al. (LMC) sample. L/C(SiC) is the integrated L/C ratio of the SiC feature (Section 6).

on the Galactic and SMC sample of Sloan et al. (2006) as well as our LMC sample (Zijlstra et al. 2006). Sloan et al. (2006) find weaker SiC and MgS features in the SMC than in the Galaxy, related to the lower abundance of Si, S and Mg in the SMC.

Our SMC sample confirms that the strength of the SiC feature is lower in the SMC than in the LMC and the Galaxy. However, there are two noticeable exceptions from the Sloan et al. sample (filled triangles).

The distribution of strength with colour (optical depth) is fundamentally different in the Galaxy compared to the SMC. In the SMC, there is a clear trend of increasing SiC strength with optical depth (left-hand panel of Fig. 12). In the Galaxy, SiC increases rapidly up to [6.4]–[9.3] $\approx$ 0.5, followed by a decline towards the SMC relation. The difference in the Galactic and Magellanic Cloud distributions is very clear in the right-hand panel of Fig. 12. Note that one SMC star follows the Galactic sample: GM 780 located outside of the scale of the left-hand panel (and therefore not shown). This object (see Section 5.2) has a strong SiC feature but with an unusual shape and rather weak dust continuum. We return to it below.

The rapid increase of SiC L/C ratio for Galactic stars at very low [6.4]–[9.3] colour (Fig. 12) suggests that in the Galaxy, the SiC feature is present while the dust excess is still low. The subsequent decline in L/C ratio may include effects of optical depth within the feature (Speck, Thompson & Hofmeister 2005), or it may be due to the increasing dust continuum. The LMC stars increase much more slowly with optical depth, and reach the peak around [6.4]–[9.3] $\approx$ 1.0; redward they are close to or a little below the Galactic stars. For the SMC stars, there is no well-defined peak but most SMC stars with [6.4]–[9.3] $<$ 1.0 have little or no SiC.

9.2 Condensation sequence

The difference between the SMC and the Galaxy can be understood if for Galactic stars, SiC condenses at similar temperatures to carbon dust. For the LMC stars, SiC occurs a bit later, while for the SMC stars, SiC forms last. Thus, there is a shift in condensation sequence over this range in metallicity.

The condensation temperature of graphite is around 1600 K whilst for SiC $T_c \approx 1400$ K. In consequence, SiC will condense slightly later in the stellar wind. Indeed, pre-solar graphite grains show no evidence of graphite coatings (as would be expected if they form earlier), whilst other condensates such as TiC, which form at higher temperature than graphite, do show coatings (Croat, Staderman & Bernatowicz 2005). However, there appears to also be an evolutionary effect, since SiC grains show less evidence for s-process enrichment, while graphite grains are highly enriched, suggesting less evolved stars show relatively less graphite more SiC (Croat et al. 2005).

The condensation temperatures are composition and density dependent. For high partial pressure, condensation occurs at higher temperatures. The effect is shown by Bernatowicz et al. (2005). For decreasing C/O ratio, graphite condenses at lower T. With increasing Si abundance, T_c (SiC) will increase. SiC and graphite can condense at similar temperatures (slightly lower for SiC), requires high density, low C/O ratio ($<$1.1) and high Si abundance. Fig. 12 suggests these conditions are met for Galactic stars. For LMC stars, SiC condensation is delayed, while for SMC stars in many cases SiC does not condense at all. The increasing C/O ratio also aids this process. Chigai & Yamamoto (2003) also suggest that under different conditions, either SiC and graphite may form together, only SiC grains may form or only graphite forms.

Following this, we interpret GM 780 as a case where the density in the dust formation region is so high and/or the C/O ratio is so low that only SiC forms. This is clearly an unusual set of conditions in the SMC. The relatively blue Manchester colour of this object is due to the resulting lack of dust. The lack of clear C_2H_2 features is also consistent with this interpretation. In the Galaxy SiC grains may come from less evolved carbon stars (Croat et al. 2005), suggesting such stars show similar conditions to GM 780.

9.3 Central wavelength

Fig. 13 shows the apparent central wavelength of the SiC feature as a function of the [6.4]–[9.3] colour. The right-hand panel displays our measurements together with the other samples mentioned above. Our sample shows that for the stars with [6.4]–[9.3] $<$ 0.5, there is a clear trend of decreasing central wavelength with increasing colour, while the opposite is observed for redder stars. The dashed line shows the fit proposed for Galactic stars (Sloan et al. 2006).

This shift could be due to two factors (Zijlstra et al. 2006). The broad C_2H_2 absorption band centred at 13.7 μm is close to the SiC feature and the red continuum wavelengths we use for SiC necessarily fall within this band. Thus stronger C_2H_2 absorption shifts the

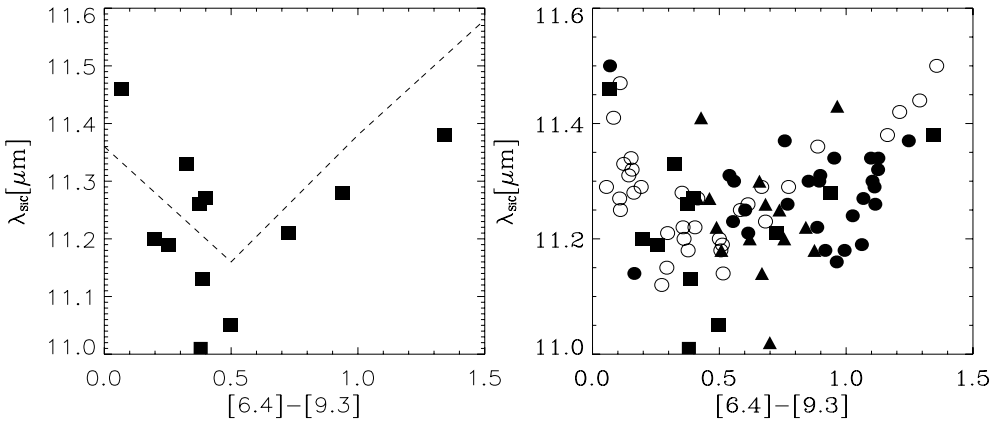

Figure 13. Apparent central wavelength of the SiC feature as a function of the [6.4]–[9.3] colour. Left-hand panel: our SMC sample. Right-hand panel: filled squares represent our SMC sample, triangles represent Sloan et al. (SMC) sample, open circles represent Sloan et al. (Galactic) sample and filled circles represent Zijlstra et al. (LMC) sample. The dashed line is the fit for Galactic stars (Sloan et al. 2006).

SiC central wavelength to the red. Speck et al. (2005) also suggested that self-absorption of SiC can also induce a shift towards the red of the SiC feature.

The shape of the SiC feature appears to be the same for all stars (e.g. Zijlstra et al. 2006). This argues against wavelength-dependent optical depth effects (Speck et al. 2005) for our samples. We note that the stars studied here have relatively low optical depth compared to stars with known SiC absorption.

10 MAGNESIUM SULFIDE

Longward of 15 μm, only the MgS feature is seen. The shape of this feature is similar in the SMC and the LMC. Furthermore, we have shown (Section 4.1) that this feature is present in the envelopes of the reddest stars, i.e. the stars with the lowest dust temperature. This is explained by the formation process of MgS which starts around 600 K and is complete around 300 K.

The feature is only seen for two stars in the SMC sample, but this appears to be due to the dust temperatures. Fig. 14 shows the comparison between the SMC and the LMC. There is little difference between them, and it appears the ratio between MgS and carbon dust is less sensitive to the metallicity than is the SiC versus carbon dust. This may indicate that the MgS condensation is limited by the available dust surface rather than the element abundances.

The shape of the continuum subtracted MgS feature is shown in Fig. 15. The MgS band of NGC 419 MIR 1 has a relatively flat shape, while the band observed in IRAS 00554−7351 diminishes towards the red. These shapes are similar to the shapes of the MgS features observed in the LMC (Zijlstra et al. 2006). The study of this feature in Galactic sources has shown that it could be resolved in two subpeaks centred at 26 and 33 μm (Volk et al. 2002). Those subpeaks are not observed in our sample, but this is not conclusive due to the low signal.

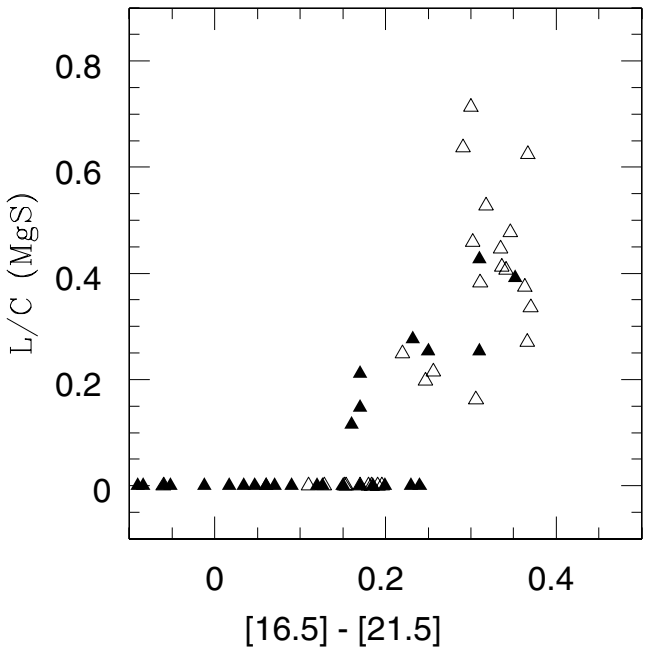

Figure 14. Strength of the MgS feature versus [16.5]–[21.5] colour. Filled triangles: SMC stars (present sample and Sloan et al. 2006); open triangles: LMC stars (Zijlstra et al. 2006). The band strength is defined as the integrated line-to-continuum ratio (Section 6). L/C(MgS) is the integrated L/C ratio of the MgS feature (Section 6).

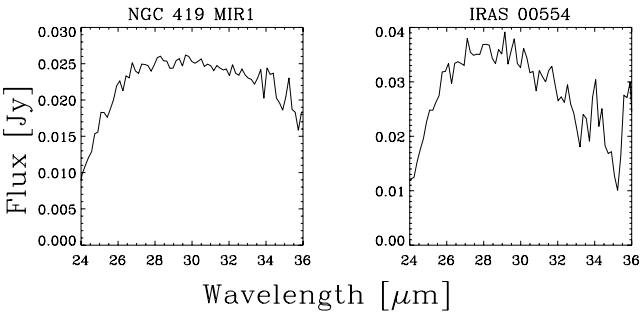

Figure 15. Shape of the MgS feature, continuum subtracted, for SMC carbon-rich AGB stars.

11 GAS PROPERTIES

11.1 C_2H_2

Fig. 16 shows the equivalent width of the C_2H_2 band at 7.5 μm for SMC, LMC and Galactic stars. Because of a lower dust-to-gas ratio at lower metallicity, stars with the same gas mass-loss rate will have a lower optical depth in the SMC than in the LMC and the Galaxy. If we use the [6.4]–[9.3] colour as a tracer of the *dust* mass-loss rate, the strength of the 7.5-μm band is comparable in the Galactic sample and our SMC sample. However, the [6.4]–[9.3] colour will be different for a given *gas* mass-loss rate. Zijlstra et al. (2006) show that the effect of metallicity on the optical depth (lower metallicity stars have lower optical depth) is stronger for redder stars (see fig. 10 in their paper). Most of the SMC stars in our sample have [6.4]–[9.3] < 0.4. To be compared with stars with similar gas mass-loss rates, we should, according to the previous work, compare those stars with stars with [6.4]–[9.3] ≈ 0.5 and 0.6 in the LMC and the Galaxy, respectively.

By applying this shift, we observe that the 7.5-μm feature is stronger in the SMC than in the LMC and the Galaxy. This feature appears to be stronger in lower metallicity environments. This has previously been found for the LMC (Matsuura et al. 2006; Zijlstra et al. 2006) and the SMC (Sloan et al. 2006). The stars in our sample are bluer than the previous observed stars, and we confirm that the C_2H_2 feature is stronger in low metallicity environments even when the stars are almost naked stars.

As noticed before in the LMC and SMC, this effect is more clearly seen for the 7.5-μm feature than for the 13.7-μm one.

The divided spectra in Fig. 11 present absorption bands at 7.4 and 13.7 μm. This confirms that the C_2H_2 features are stronger in the SMC than in the LMC.

Fig. 17 shows a trend of increasing C_2H_2 strength with increasing SiC strength in the SMC. Such a trend is also observed in the LMC but the slope is different. Whether this trend is present for the Galaxy is less obvious. This is corroborated by a study of Galactic AGB stars *Spitzer* Low Resolution Spectrometer (LRS) spectra that shows no correlation between any molecular bands and the strength of the SiC feature (Thompson et al. 2006). The SiC condensation sequence discussed above is consistent with this: in the Galaxy, SiC is limited by Si, and in the Magellanic Clouds by the C/O ratio. This predicts a correlation with C_2H_2 only for the Magellanic Clouds.

The distribution in Fig. 17 clearly shows a separation into SMC–LMC–Galaxy, from left to right. The ratio of C_2H_2 (gas) over SiC (dust) is higher in the SMC, than in the LMC and the Galaxy. This shows an increasing gas-to-SiC dust mass ratio with decreasing metallicity.

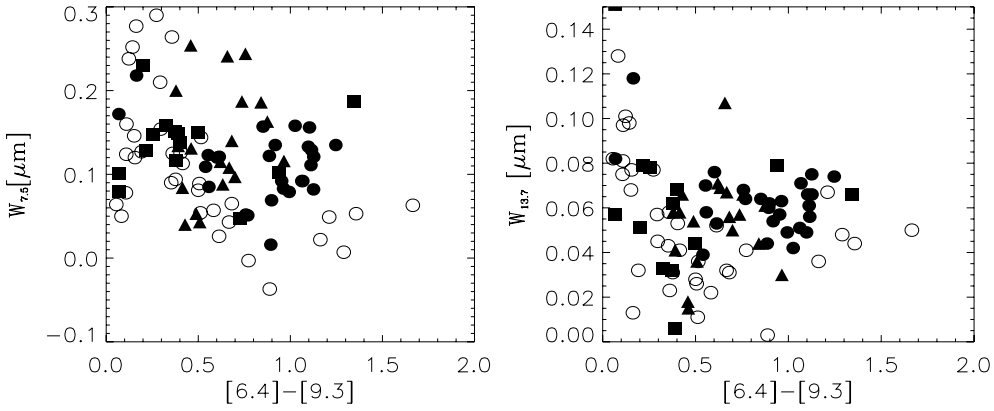

Figure 16. The equivalent width of the C_2H_2 band at 7.5 μm (left) and 13.7 μm (right) as a function of the [6.4]–[9.3] colour. Filled squares represents our SMC sample, triangles represent the Sloan et al. SMC sample, open circles represent the Sloan et al. Galactic sample and filled circles represent the Zijlstra et al. LMC sample.

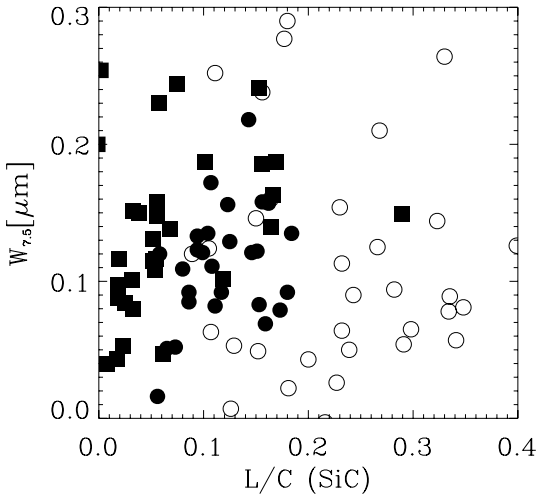

Figure 17. The strength of the C_2H_2 7.5 μm feature as a function of the SiC feature. Squares represent SMC stars from our sample and Sloan et al. sample, black circles represent the Zijlstra et al. LMC sample and open circles represent the Sloan et al. Galactic sample.

11.2 CO

In all the spectra, the flux drops sharply shortward of 6 μm. This is due to absorption by the CO molecule (Jørgensen et al. 2000), C_2 and/or C_3 (Zijlstra et al. 2006), as shown by the spectra at the top of Fig. 3. The slope of this feature is steeper in the LMC than in the SMC. We attribute this to an underabundance of CO in the SMC with respect to the LMC. For carbon stars, the CO abundance is limited by oxygen. Oxygen is a measure for the original metallicity: the CO band is therefore expected to vary with metallicity. Note that the responsivity at the blue edge of the spectra is low.

12 CARBON VERSUS OXYGEN-RICH STARS

A noticeable finding for both the LMC and the SMC is that the *Spitzer* targets are found to be strongly biased towards carbon stars. The selection criteria were relatively insensitive to the chemical type, and the bias is therefore intrinsic rather than a selection effect. Apart from stars observed as a result of acquisition errors, we found 14 carbon stars and no oxygen-rich stars.

Sloan et al. (2006) use 2MASS colours as part of their selection criteria. This gave a sample of 22 carbon stars versus 10 oxygen-rich stars (excluding some other sources). The use of 2MASS requires low circumstellar reddening and favours stars with silicate dust where the reddening per unit dust mass is lower.

The LMC sample of Zijlstra et al. (2006) shows 28 carbon stars versus one oxygen-rich star (excluding one high-mass proto-star). Buchanan et al. (2006) observed high-luminosity stars and found 16 C-rich versus four O-rich AGB stars. Thus, the dominance of carbon stars is confirmed in all surveys of mass-losing stars, but the ratio depends on the characteristics of the survey. The proportion of C stars is lower in high luminosity, lower optical depth surveys.

Cioni & Habing (2003) show that for optically visible evolved stars in the Magellanic Clouds, the ratio of C over M stars is approximately 3 for both clouds. Blum et al. (2006) surveying the full population of AGB stars in the LMC, identify 17 500 O-rich and 7000 C-rich stars. The higher ratio of O to C stars found by Blum et al. may suggest that they include K-type stars, earlier on the AGB. Cioni & Habing (2003) estimate that there are about 2250 C stars in the SMC and 10 000 in the LMC, the latter being roughly consistent with the Blum et al. numbers.

The high ratio (∼3) of C- to O-rich stars is consistent with the expectation that in the Magellanic Clouds most stars become carbon stars early on the AGB, before the onset of the high mass-loss rate phase. There are almost no O-rich stars in the present and the Zijlstra et al. (2006) samples of lower luminosity, high mass-loss rate, AGB stars in the Magellanic Clouds. Only among the highest mass, higher luminosity stars on the AGB do O-rich stars contribute significantly to the population of mass-losing stars.

12.1 Carbon star evolution

Fig. 6 shows that in the LMC, the carbon star luminosity function exhibits a flat peak with a width of 0.3 mag. This traces the part of the AGB evolution where essentially all stars have become carbon stars: the flat distribution results from the linear change of magnitude with time. (Stars more massive than ∼4 $M_\odot$ may avoid a carbon star phase due to hot bottom burning, but there are few such stars.) At the high-luminosity end, the number of known stars drops because of increasing obscuration and stars leaving the AGB.

In the SMC, the width of the flat peak is about 0.6 mag. Over 10^6 yr, a star brightens by approximately 1 mag on the AGB. These numbers therefore predict that the optical carbon star phase lasts

3×10^5 to 6×10^5 yr, for the LMC and the SMC, respectively. These are lower limits to the total lifetime of the carbon star phase on the AGB.

The SMC carbon star distribution peaks at lower luminosity than in the LMC. The longer lifetime in the SMC is therefore due to the stars becoming carbon-rich earlier, after fewer thermal pulses.

The *Spitzer* targets all are at the high-luminosity end, and trace the final stage of their evolution. The Manchester colours of the SMC stars indicates mass-loss rates of $10^{-5}\,M_\odot\,yr^{-1}$ or higher (Zijlstra et al. 2006, their fig. 10). Assuming that a typical carbon star expels $0.2\,M_\odot$ during the superwind, indicates a duration of this phase of order $\sim 10^4$ yr. The combined SMC samples have approximately 30 superwind stars, or roughly 1 per cent of the total number of carbon stars predicted by Cioni & Habing (2003). This suggests a lifetime of the carbon star phase of $\sim 10^6$ yr. For comparison, the thermal-pulsing AGB lasts $1–2 \times 10^6$ yr for $1–3\,M_\odot$ stars. Thus, SMC stars become carbon stars during the first half of the thermal-pulsing phase.

12.2 Mass loss and metallicity

A clear result from the *Spitzer* surveys is the enhancement of C_2H_2 in low-metallicity environments. This has previously been found from ground-based spectra. van Loon et al. (1999a) and Matsuura et al. (2002, 2005) argue that this is related to a higher C/O ratio in these stars. The C/O ratio is enhanced by two effects: (i) a lower oxygen abundance means that less carbon is locked up in CO (e.g. Lattanzio & Wood 2003), and (ii) lower metallicity promotes more efficient third dredge-up of carbon (Wood 1981; Vassiliadis & Wood 1993) with stars experiencing more thermal pulses (Lawlor & MacDonald 2006).

This seems to be confirmed by the finding that LMC carbon stars have higher abundances of C_2H_2 than Galactic stars. In contrast, oxygen-rich stars show low molecular abundances at low metallicity (Zijlstra 2006).

Spitzer shows that in the LMC and SMC, high mass-loss stars are heavily dominated by carbon stars, unlike in the Galaxy (Blum et al. 2006; Buchanan et al. 2006; Sloan et al. 2006; van Loon et al. 2006; Zijlstra et al. 2006; this paper). In contrast, the sole oxygen-rich AGB star in the sample of Zijlstra et al. has a rather moderate mass loss. Only the most luminous LMC stars show an O-rich population with thick dust shells.

This leads to the suggestion that at low metallicity, stellar mass loss is mostly carbon rich, as at the luminosity where stellar pulsations develop an extended atmosphere leading to molecule and dust formation, the stars have already become carbon rich. Only in old stellar systems (globular clusters, Galactic halo), where the stellar masses are insufficient for third dredge-up, is an oxygen-rich wind expected.

The lack of silicon implies that the dust input into the interstellar medium (ISM) from LIMS in low metallicity systems would be lacking in silicates and silicate carbides, but be dominated by carbonaceous dust (Matsuura et al. 2006; Zijlstra 2006; Groenewegen et al., in preparation).

13 CONCLUSION

We have presented a *Spitzer* spectroscopic survey of 14 carbon-rich AGB stars in the SMC. The bolometric magnitudes of the observed stars indicates that their initial masses are in the range $1–4\,M_\odot$. We also presented spectra of an accidentally observed K supergiant and an H II region.

Our spectra covers the range 5–38 μm. Molecular bands due to C_2H_2 at 7.5 and 13.7 μm are observed in most of the C-rich stars. A weak absorption band at 14.3 μm, attributed to HCN, is observed in the two reddest stars of our sample. The 5.8-μm band of carbonyl observed in the LMC is not observed in our SMC sample. This could be due to an underabundance of CO in the SMC with respect to the LMC. The acetylene bands provide clear evidence for a higher C/O ratio in low metallicity carbon stars.

Using the 'Manchester System', we determined the continuum flux for the observed stars using four narrow bands centred at 6.4, 9.3, 16.5 and 21.5 μm. This enables us to determine two colour temperatures, [6.4]–[9.3] and [16.5]–[21.5]. These colours are indicators of the optical depth and dust temperatures, respectively.

We find evidence for a different behaviour of the SiC feature with metallicity: in the Galaxy, it first appears in stars showing a hot dust excess, while for the SMC it only appears for stars with cool dust. The LMC is intermediate. We suggest that this is due to a shift in the formation sequence, where at solar metallicity SiC closely follows graphite, while at SMC metallicity and its corresponding higher C/O ratio, graphite forms earlier, and SiC much later do to the lower Si abundance.

The MgS feature at ∼30 μm has strength comparable to LMC stars, suggesting its abundance relative to that of amorphous carbon is less metallicity dependent. We suggest its formation is limited by the available surface area of pre-existing dust grains, rather than elemental abundances. The shape of the MgS and SiC features are similar in both galaxies, but the SiC feature is much stronger in the LMC than in the SMC.

We show that a colour–colour diagram using *Spitzer* IRAC and MIPS filters ([5.8]–[8.0] versus [8.0]–[24]) is able to separate O-rich and carbon stars. This had been shown by Buchanan et al. (2006) for redder stars; we confirm that it is also valid for blue stars ([8]–[24] < 3). Furthermore, we show that this separation is independent of metallicity. This suggests that it is possible to discriminate C- and O-rich AGB stars in other galaxies using only *Spitzer* photometry.

Carbon stars dominate the population of high mass-loss rate AGB stars in the SMC. We derive a lifetime of the carbon star phase of $\gtrsim 6 \times 10^5$ yr, with the superwind phase lasting $\sim 10^4$ yr. Thus, stars become carbon-rich early on the thermal-pulsing AGB, long before the onset of the superwind. The LMC stars become carbon-rich later in their evolution, and last as carbon stars for $\gtrsim 3 \times 10^5$ yr.

ACKNOWLEDGMENTS

EL acknowledges support from a PPARC rolling grant. AAZ acknowledges a Royal Society grant to allow a visit to the SAAO, and is grateful for the hospitality of the SAAO. PRW has been partially supported in this research by a Discovery Grant from the Australian Research Council.

REFERENCES

Aoki W., Tsuji T., Ohnaka K., 1999, A&A, 350, 945
Banwell C. M., McCash E. M., 1994, Fundamentals of Molecular Spectroscopy, 4th edn. McGraw-Hill, London, p. 19
Bellazzini M., Ferraro F. R., Pancino E., 2001, ApJ, 556, 635
Bernatowicz T. J., Akande O. W., Croat T. K., Cowsik R., 2005, ApJ, 631, 988
Bessell M. S., Wood P. R., Evans T. L., 1983, MNRAS, 202, 59
Blum R. D. et al., 2006, AJ, 132, 2034
Bowen G. H., Willson L. A., 1991, ApJ, 375, L53
Buchanan C. L., Kastner J. H., Forrest W. J., Hrivnak B. J., Sahai R., Egan M. P., Frank A., Barnbaum C., 2006, AJ, 132, 1890

Cernicharo J., Yamamura I., González-Alfonso E., de Jong T., Heras A., Escribano R., Ortigoso J., 1999, ApJ, 526, L41
Chandra S., Kegel W. H., Le Roy R. J., Hertenstein T., 1995, A&AS, 114, 175
Cherchneff I., 2006, A&A, 456, 1001
Chigai T., Yamamoto T., 2003, Geochim. Cosmochim. Acta, 67, A64
Cioni M.-R., Habing H. J., 2003, A&A, 402, 133
Cioni M.-R. L. et al., 2003, A&A, 406, 51
Costa E., Frogel J. A., 1996, AJ, 112, 2607
Croat T. K., Staderman F. J., Bernatowicz T. J., 2005, ApJ, 631, 976
de Freitas Pacheco J. A., Barbuy B., Idiart T., 1998, A&A, 332, 19
Dray L. M., Tout C. A., Karakas A. I., Lattanzio J. C., 2003, MNRAS, 338, 973
Egan M. P., Van Dyk S. D., Price S. D., 2001, AJ, 122, 1844
Goorvitch D., 1994, ApJS, 95, 535
Groenewegen M. A. T. et al., 2007, MNRAS, in press (doi: 10.1111/j.1365-2966.2007.11428.x)
Harris G. J., Polyansky O. L., Tennyson J., 2002, ApJ, 578, 657
Harris G. J., Tennyson J., Kaminsky B. M., Pavlenko Y. V., Jones H. R. A., 2006, MNRAS, 367, 400
Hony S., Waters L. B. F. M., Tielens A. G. G. M., 2002, A&A, 390, 533
Houck J. R. et al., 2004, ApJS, 154, 18
Jørgensen U. G., Hron J., Loidl R., 2000, A&A, 356, 253
Keller S. C., Wood P. R., 2006, ApJ, 642, 834
Kontizas E., Dapergolas A., Morgan D. H., Kontizas M., 2001, A&A, 369, 932
Lattanzio J. C., Wood P. R., 2003, in Habing H. J., Olofsson H., eds, Astron. Astrophys. Library, Asymptotic Giant Branch Stars. Springer, Berlin
Lawlor T. M., MacDonald J., 2006, MNRAS, 371, 263
Lloyd Evans T., 1980, MNRAS, 193, 87
Lloyd Evans T., Glass I. S., Catchpole R. M., 1988, MNRAS, 231, 773
Maeder A., 1992, A&A, 264, 105
Matsuura M., Zijlstra A. A., van Loon J. Th., Yamamura I., Markwick A. J., Woods P. M., Waters L. B. F. M., 2002, ApJ, 580, L133
Matsuura M. et al., 2005, A&A, 434, 691
Matsuura M. et al., 2006, MNRAS, 371, 415
Murphy M. T., Bessell M. S., 2000, MNRAS, 311, 741
Pietrinferni A., Cassisi S., Salaris M., Castelli F., 2006, ApJ, 642, 797
Prévot L., Martin N., Rebeirot E., Maurice E., Rousseau J., 1983, A&AS, 53, 255
Querci F., Querci M., Kunde V. G., 1971, A&A, 15, 256
Rebeirot E., Azzopardi M., Westerlund B. E., 1993, A&AS, 97, 603
Renzini A., 1981, Astrophys. Space Sci. Library, 89, 319
Sloan G. C., Neremberg P. S., Russel M. R., 2003, IRS Technical Report 03001
Sloan G. C., Kraemer K. E., Matsuura M., Wood P. R., Price S. D., Egan M. P., 2006, ApJ, 645, 1118
Speck A., Thompson G. D., Hofmeister A., 2005, ApJ, 634, 426
Speck A. K., Cami J., Markwick-Kemper C., Leisenring J., Szczerba R., Dijkstra C., Van Dyk S., Meixner M., 2006, ApJ, 650, 892
Tanabe T. et al., 1997, Nat, 385, 509
Thompson G. D., Cormon A. D., Speck A. K., Dijkstra C., 2006, ApJ, 652, 1654
van Loon J. Th., 2006, in Lamers H., Langer N., Nugis T., Annuk K., eds, ASP Conf. Ser. Vol. 353, Stellar Evolution at Low Metallicity: Mass Loss, Explosions, Cosmology. Astron. Soc. Pac., San Francisco, p. 211
van Loon J. Th., Zijlstra A. A., Groenewegen M. A. T., 1999a, A&A, 346, 805
van Loon J. Th., Groenewegen M. A. T., de Koter A., Trams N. R., Waters L. B. F. M., Zijlstra A. A., Whitelock P. A., Loup C., 1999b, A&A, 351, 559
van Loon J. Th., Marshall J. R., Zijlstra A. A., 2005, A&A, 442, 597
van Loon J. Th., Marshall J. R., Cohen M., Matsuura M., Wood P. R., Yamamura I., Zijlstra A. A., 2006, A&A, 447, 971
Vassiliadis E., Wood P. R., 1993, ApJ, 413, 641
Volk K., Kwok S., Hrivnak B. J., Szczerba R., 2002, ApJ, 567, 412
Wachter A., Schröder K.-P., Winters J. M., Arndt T. U., Sedlmayr E., 2002, A&A, 384, 452
Werner M. W., Uchida K. I., Sellgren K., Marengo M., Gordon K. D., Morris P. W., Houck J. R., Stansberry J. A., 2004, ApJS, 154, 1
Westerlund B. E., Azzopardi M., Rebeirot E., Breysacher J., 1991, A&AS, 91, 425
Whitelock P. A., Feast M. W., Menzies J. W., Catchpole R. M., 1989, MNRAS, 238, 769
Whitelock P. A., Feast M. W., Marang F., Groenewegen M. A. T., 2006, MNRAS, 369, 751
Woitke P., 2006, A&A, 460, L9
Wood P. R., 1981, Astrophys. Space Sci. Library, 88, 135
Zijlstra A. A., 2004, MNRAS, 348, L23
Zijlstra A. A., 2006, in Barlow M. J., Mendez R. H., eds, Proc. IAU Symp. 231, Planetary Nebulae in our Galaxy and Beyond. Cambridge Univ. Press, Cambridge, p. 55
Zijlstra A. A. et al., 2006, MNRAS, 370, 1961

This paper has been typeset from a TEX/LATEX file prepared by the author.